RSC Applied Interfaces

ROYAL SOCIETY OF CHEMISTRY

PAPER

View Article Online
View Journal

Cite this: DOI: 10.1039/d5lf00339c

A self-powered (In,Ga)N biosensor with Au nanoparticles for monitoring live cell activities

Linrui Cheng,†[ab] Qianyi Zhang,†[b] Binbin Hou,[ab] Zixun Wang,*[ac] Yibin Wang,[d] Jianya Zhang*[d] and Yukun Zhao *[abe]

Received 4th November 2025,
Accepted 10th June 2026

DOI: 10.1039/d5lf00339c

rsc.li/RSCApplInter

The use of biosensors to detect cell activities is of great significance for understanding their biological functions and drug responses. In this work, we propose a self-powered (In,Ga)N biosensor without an external power supply, which is capable of label-free monitoring of live cell activities. Based on the electrical conductivity, Au nanoparticles are deposited on the surface of the (In,Ga)N layer to help cells to adhere to the sensor. Thanks to its small size and continuous monitoring, the biosensor enables us to capture the dynamics of cell adhesion-based activities *in situ*. In addition, it is found that Au nanoparticles can enhance the current intensity significantly, which could accelerate the electron transfer between the electrodes or increase the reactive oxygen species in cells. According to the spike signals, the biosensor can make contact with live cells for detecting cell activities. Therefore, this developed self-powered biosensor provides a new method to study the cell activities *in situ* with ultralow power consumption.

1. Introduction

A biosensor functions as a detection tool capable of identifying biomolecules and transforming their levels into signals like light and electricity. It combines biometric components and signal conversion components to achieve the conversion and transmission of biological signals.[1–5] As the analytical speed, sensitivity and selectivity of biosensors have increased, they have started to move toward automation, miniaturization and integration.[6–8] They are valuable in various fields, including biology, medicine, food and environmental detection.[2,9] Among them, cell-based biosensors have a broad range of detection capabilities since they can directly monitor the physiological characteristics of live cells and study the effects of drugs.[10,11] With the advancement of materials science and nanotechnology, attempts have been made to adapt nanomaterials to biosensors.[12–14] With good compatibility, the biosensors using nanomaterials have the advantages of maintaining cell activities, promoting electron transfer between electrodes and biomolecules, improving sensitivity and response time, *etc.*[2,12,15,16] They can also detect biomolecules label-free, accelerating the pace of diagnosis.[17] In addition, self-powered biosensors that do not require an external power source have also attracted widespread attention in biological analysis due to their advantages such as being easier to miniaturize.[18–20]

Semiconductor materials can produce substances or messages by sensing signals from cells, such as electrons, metabolites or biomolecules. They have also been employed in the creation of biosensors and are capable of achieving a variety of signal transduction pathways at biological interfaces.[21] As a wide bandgap semiconductor, gallium nitride (GaN) has drawn enormous attention because of its superior chemical and physical characteristics.[22,23] Compatibility, coupling, energy conduction and other aspects must be taken into account when applying it to biosensors based on cells.[1] Hou *et al.* applied a single device to quantitatively detect the progress of different intracellular processes,[24] which required an external power source to drive the LED to emit light. In addition, Au nanoparticles (NPs) have been proven to have good biocompatibility, electron conduction, catalysis and other properties.[25–28] However, a self-powered (In,Ga)N biosensor with Au nanoparticles

[a] *School of Nano-Tech and Nano-Bionics, University of Science and Technology of China, Hefei 230026, China*
[b] *Key Laboratory of Semiconductor Display Materials and Chips, Suzhou Institute of Nano-Tech and Nano-Bionics (SINANO), Chinese Academy of Sciences (CAS), Suzhou 215123, China. E-mail: ykzhao2017@sinano.ac.cn*
[c] *Jiangsu Key Laboratory of Organoid Engineering and Precision Medicine, SINANO, CAS, Suzhou 215123, China. E-mail: zixunwang2021@sinano.ac.cn*
[d] *Key Laboratory of Intelligent Optoelectronic Devices and Chips of Jiangsu Higher Education Institutions, School of Physical Science and Technology, Suzhou University of Science and Technology, Suzhou 215009, China. E-mail: jyzhang2022@usts.edu.cn*
[e] *Guangdong Institute of Semiconductor Micro-Nano Manufacturing Technology, Foshan 528225, China*
† These authors contributed equally to this work.

has not yet been applied in monitoring live cell activities.

In our previous studies, we studied the preparation and properties of GaN and (In,Ga)N materials.[29,30] In this work, we propose a self-powered (In,Ga)N biosensor with Au nanoparticles for monitoring live cell activities. Self-power refers to the sensor working without the need for external power sources.[19] By depositing Au NPs on the surface of the film, it is found that the current signal is enhanced significantly, indicating the activities of live cells. The underlying mechanisms have also been discussed. Notably, the biosensor is capable of self-powered detection. Therefore, (In,Ga)N-based biosensors coated with Au NPs on the surface can be used for monitoring of cell activities.

2. Experimental section

2.1 Preparation of the (In,Ga)N wafer

The structure of the (In,Ga)N film epitaxial wafer is shown in Fig. 1a–c. We first used metal organic chemical vapor deposition (MOCVD) to epitaxially grow the (In,Ga)N based epitaxial structure on the silicon (Si) substrate. Following the growth direction, the epitaxial structure included a Si-doped n-GaN layer, (In,Ga)N/(Al,Ga)N multiple quantum wells (MQWs), a p-(Al,Ga)N layer, and a p-GaN contact layer.

2.2 Preparation of the biosensors

After the completion of MOCVD growth, 6 nm Au NPs were deposited on the surface. The sample was divided into small pieces of 10 mm × 10 mm and subjected to ultrasonic cleaning. The (In,Ga)N film epitaxial wafer was then subjected to the surface hydrophilicity treatment. It was placed in a plasma adhesive remover and treated in pure oxygen at 200 °C for 5 min. After that, the melted Pb/Sn alloys were applied to the Si substrate surface and an electric wire was connected. The electric wire was sealed with the epoxy resin and heated in order to cure them. The (In,Ga)N film epitaxial wafer was sent to the cell chamber for cell implantation. After 24 hours, the (In,Ga)N film epitaxial wafer with the cells on the surface was taken out. The cells used for testing were HCT-116.

2.3 Characterization and measurement methods

We tested the biosensor using an electrochemical workstation (DH7000) to confirm its ability to detect cell activity. The entire testing process of the experiment was conducted under ambient lighting conditions without any additional light sources. The characterization instrument used is high-resolution high-angle annular dark-field scanning transmission electron microscopy (HAADF-STEM, Talos F200X, FEI) with high-resolution energy-dispersive X-ray (EDX) imaging. In order to characterize the morphology

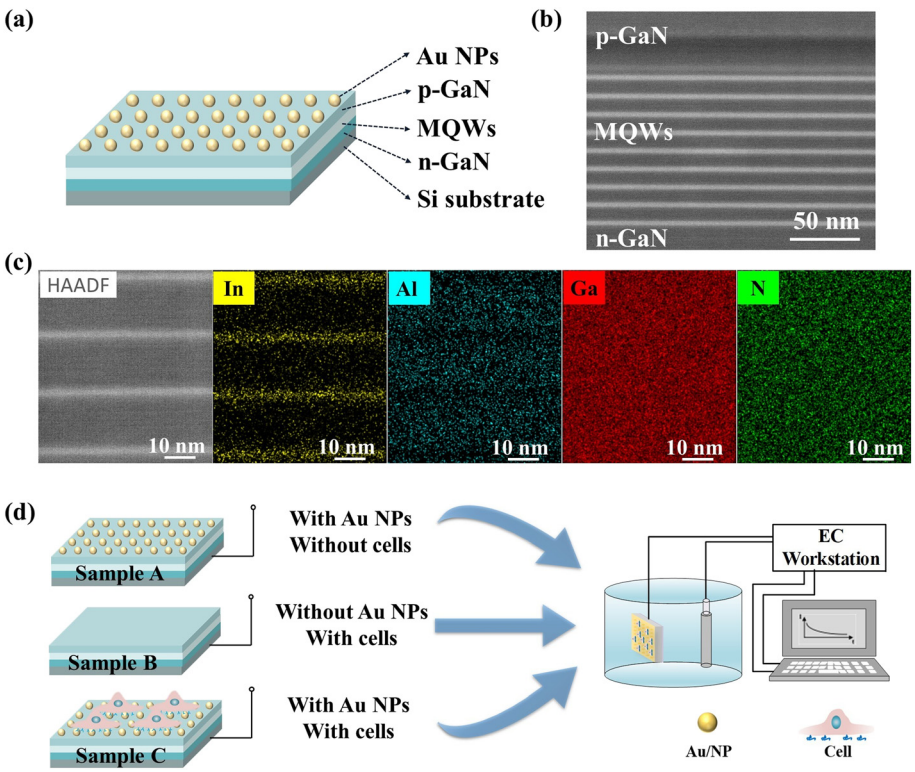

Fig. 1 (a) (In,Ga)N epitaxial layer coated with Au NPs on the surface. (b) HAADF-STEM image of the active region. (c) Enlarged HAADF-STEM images of partial MQWs, accompanied with energy dispersive spectrum (EDS) mapping of In, Al, Ga and N elements. (d) Schematic diagram of electrochemical testing.

Table 1 Overview of the samples used in this work

Biosensors	With Au NPs	With cells
Sample A	Yes	No
Sample B	No	Yes
Sample C	Yes	Yes

of cells on the device surface, this study was conducted using scanning electron microscopy (SEM, S-4800, HITACHI). Focused ion beam (FIB) was utilized to prepare STEM samples.

3. Results and discussion

Fig. 1b and c visually display the distribution of In, Al, Ga and N elements within the (In,Ga)N/(Al,Ga)N MQWs, which agree with the epitaxial design. Such a clear (In,Ga)N/(Al,Ga)N interface observed in the HAADF-STEM image is the testimony of a good crystallinity. To test the adhesion of cells on the device, we conducted a comparative experiment as shown in Fig. 1d and Table 1. Biosensor sample A is added with Au NPs, but no cells are added. Sample B has no Au NPs, but cells have been added. Biosensor sample C is added with both Au NPs and cells. The biosensors reconnected to the electrochemical workstation as the anode, and a Pt plate serves as the cathode. They form a circuit together with the solution in the electrolytic cell. We detect the process of cell adhesion by testing the current changes in this circuit. The process of cell adhesion plays an important role in the formation of tissues and organs. It is also related to physiological and pathological processes such as cell differentiation and tumor metastasis.[24]

In order to confirm that the biosensor can monitor the cell activities, the response to cell adhesion has been studied. The initial current of sample B is approximately 0.2 μA. There are no current peaks for the biosensor without Au NPs. When no cells are added, the initial current of the biosensor with plated Au NPs is significantly higher than that of the biosensor without Au NPs (Fig. S1 and 2a). This is because the modification of the electrode surface of the biosensor by Au NPs accelerates electron transfer between the electrodes. After adding HCT-116 cells, spike signals appear (Fig. 2a), which indicate that cell activity can be detected. The magnified spike signals in Fig. 2b can distinguish the cell adhesion. Ten spike signals and twenty noise signals are selected to calculate the average value. As shown in Fig. 2c, the average height of the peak signal is ~6.48 nA, which is much stronger than that of the noise signal. Fig. 2d shows the current variation trend of the cell from approaching the surface of the biosensor, starting to make contact with the biosensor, until fully contacting with the biosensor surface and fully spreading. This is the process of generating peak signals.

Fig. 3a shows that there are a considerable number of cells adhering to the surface of the biosensor. In addition, Fig. 3b and c further demonstrates the adhesion of a cell on the surface of sample C. Hence, the biosensor can make contact with live cells for detecting cell activities, whose current signals can be used for cell analysis and evaluation. Fig. 3d shows relatively obvious peak current signals. According to the electrochemical workstation, the reading

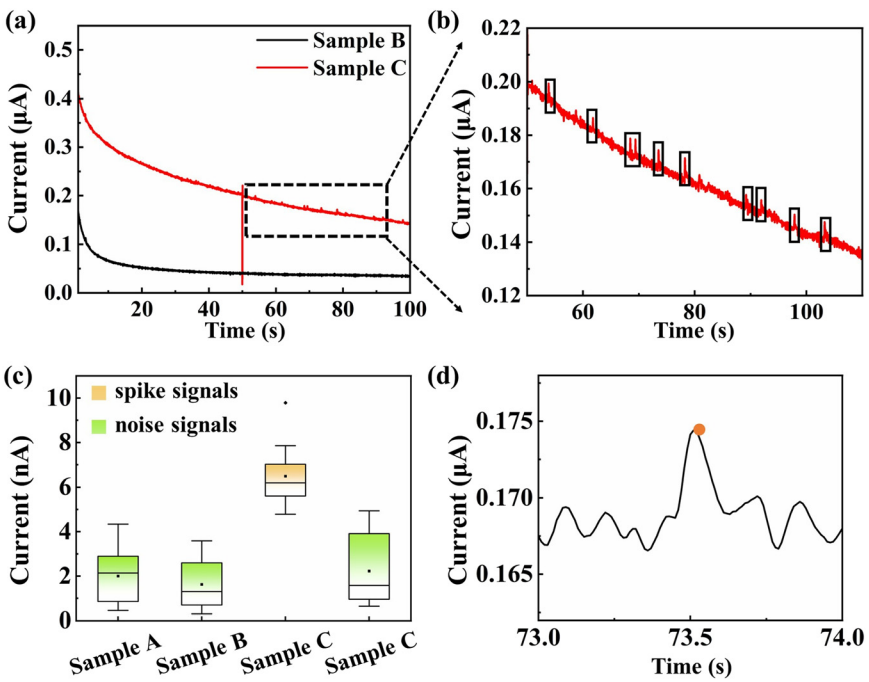

Fig. 2 (a) Current curves of samples B and C. (b) Enlarged current curve of sample C. (c) Summary statistics of spike signals and noise signals. (d) A single spike signal current diagram.

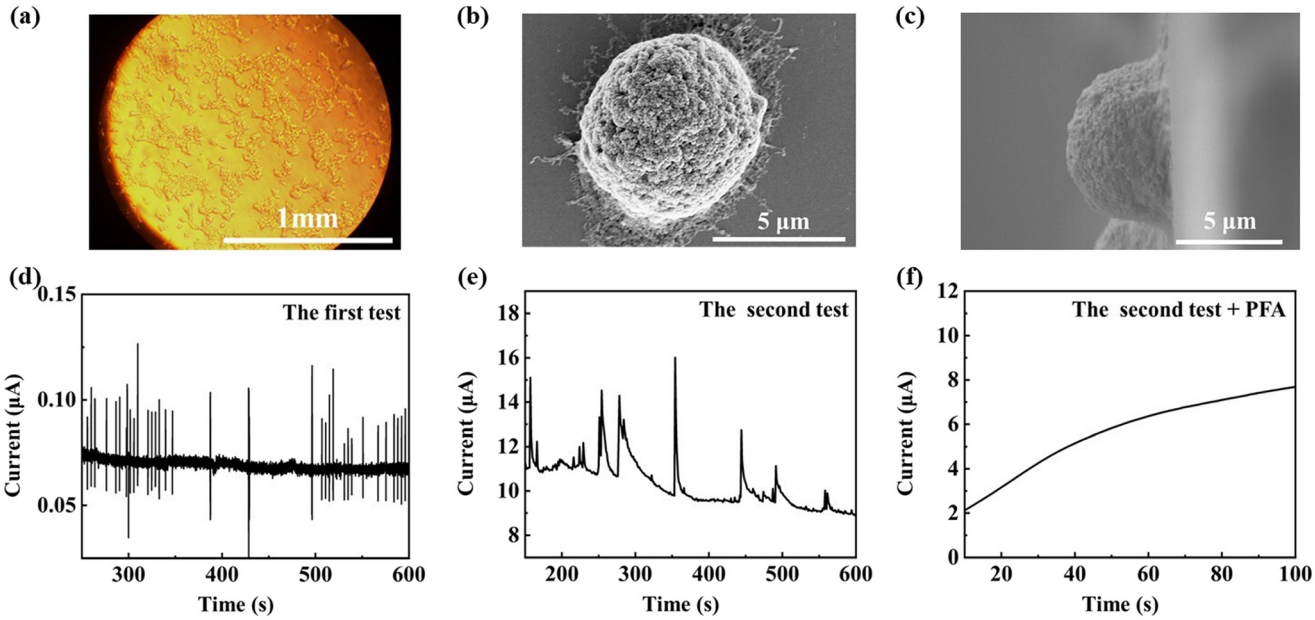

Fig. 3 (a) Cells on the surface of the biosensor observed under the optical microscope. (b) Top-view SEM image of a cell on sample C. (c) Side-view SEM image of a cell on sample C. (d) The first test of the device with Au NPs. (e) The second test of the device with Au NPs. (f) Current curve of the device after cell fixation.

time resolution of the current signal is 0.01 s. The cell concentration is approximately 2.73×10^5 cells per mL. Fig. 3e shows the results of the second test, and the clear peak current signals can still be seen. As shown in Fig. S2, clear peak current signals can still be observed during the long-term testing interval of 600 s to 1000 s. This result indicates that the device has good operational stability during long-term continuous testing. Then, we have immersed the device in a 4% paraformaldehyde (PFA) fixative for 40 minutes. Fixed dead cells are used in control experiments to compare and analyze the differences in electrical signals between live and dead cells under the same detection conditions, including the (In,Ga)N device and electrical wire connection (Fig. 3f). The results show that the fixed cells had no significant dynamic electrical response, which is quite different from the live cell group (Fig. 3e), indicating that the detection signal mainly comes from the physiological behavior of live cells (adhesion and spreading).

To further validate the specificity of peak signal generation, the 293T cells have been introduced for comparison, which have weak adhesion ability and low spreading degree.[31] The experimental result shows that 293T cells do not produce spike current signals (Fig. S3). This indicates that the current spike is not solely caused by cell physical attachment, but depends on the cell type, adhesion strength and interface electrical coupling degree, further confirming that the signal originates from the specific physiological activity of living cells. In addition, to evaluate the sensitivity and detection limit of the device, we set up 4 different concentrations of cell suspensions. In Fig. S4a–d, the cell concentrations are approximately 1.82×10^5, 9.1×10^4, 3.6×10^4 and 1.8×10^4 cells per mL, respectively. By observing the surface of the device under a microscope, visible and distinct cell adhesion can be seen. Fig. S4a shows the peak current, while no obvious peak current signals are observed in Fig. S4b–d. This may be attributed to the insufficient number of effective cells per

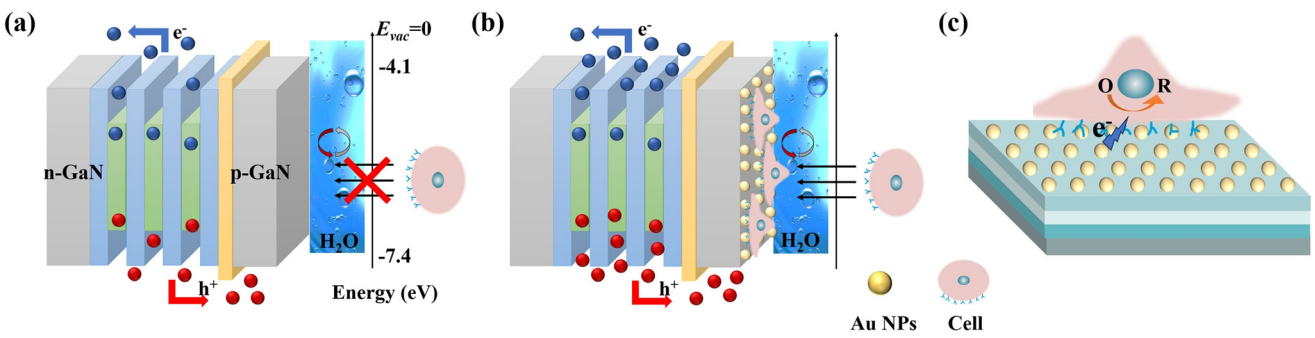

Fig. 4 Schematic diagrams of the biosensor surface (a) without Au NPs, and (b) with Au NPs. (c) The process of electron transfer between cells and the device through Au NPs.

unit area, resulting in a significant decrease in the overall electrical response intensity. Therefore, the detection threshold of the cell concentration is about 1.82×10^5 cells per mL for the detection sensitivity. Subsequently, we have conducted live/dead cell staining experiments on the cells cultured on the surface of the device (Fig. S5). The experimental results show that the cells cultured on the surface of the device exhibit bright green fluorescence, while there is almost no red fluorescence, indicating good cell viability and no significant cytotoxicity on the device surface.

To better analyze the underlying mechanisms, we plot the energy band diagrams in Fig. 4. In order to create a circuit with the external circuit and produce current, the carriers engage in oxidation–reduction reactions with the ions within the electrolytic cell (Fig. 4a). Without Au NPs, cells have difficulty adhering to the surface of the biosensor. After covering the biosensor surface with Au NPs (Fig. 4b), the current of the device significantly increases (Fig. 2a). This is because Au NPs have good conductivity, enhancing the conductivity of the electrode. After adding live cells, the cells gradually attach to the Au NPs on the biosensor surface due to the biocompatibility of Au NPs, generating current spikes (Fig. 2b). This process uses the amperometry method, which has a high temporal resolution, but cannot provide information on the chemical properties of the analyte.[32] While the working electrode maintains a constant potential, electron transfer occurs due to the potential difference between the solution and the electrode when the analyte diffuses to the electrode surface. It leads to the appearance of current spikes (Fig. 2b).

Research has shown that Au NPs can increase the reactive oxygen species (ROS) generation ability of HCT-116 cells.[33] When Au NPs collide on the surface of the cell membrane, they can cross the membrane gap and undergo electron tunneling within the cell, producing discrete current spikes.[34] These peaks may be due to the adsorption of Au NPs on the cell membrane, which drives electron tunneling through the cell membrane to produce peaks, and then leaves the cell membrane, restoring the current to the background value. The oxidation and reduction of ROS within a single cell are the causes of these spikes.[33,34] Therefore, the process of detecting current spikes caused by the contact between cells and Au NP modified semiconductor surfaces is proposed as follows, which is a working hypothesis requiring further investigation. HCT-116 cells uptake surface Au NPs, inducing an explosion of intracellular ROS. Au NPs simultaneously mediate the tunneling effect of electrons generated by intracellular ROS across the cell membrane (Fig. 4c). The tunneling electrons induced by Au NPs are injected into the p-GaN layer. When the electrons (minority carriers) are injected into the depletion region of p-GaN, the following effects occur. There are a large number of fixed acceptor negative charges in the depletion region of p-GaN. Injected electrons neutralize some negative charges, thereby reducing the width of the depletion region. The degree of band bending (*i.e.* built-in potential difference) will decrease as a result, leading to a reduction in the potential barrier. After the potential barrier is lowered, more holes (majority carriers) can be injected from the p-region to the n-region, where they undergo radiative recombination with electrons. Although this recombination process occurs in the active region of MQWs, the electrons corresponding to the recombination come from injection in the n-region, while the holes come from the p-region, leading to the synchronous enhancement of electron injection and hole injection in the MQW region. When the injection of electrons (p-region minority carriers) and the enhanced injection of holes (p-region majority carriers) occur simultaneously due to the decrease in potential barrier, a transient increase in the total forward current of the device is detected as a positive current peak.[34–38]

4. Conclusion

In this work, we develop a self-powered biosensor based on an (In,Ga)N film. This biosensor is capable of label-free monitoring of live cell activities. It requires cheap processing costs, and the preparation and testing methods of the device are simple and convenient. By altering the electrode surface of the biosensor with Au NPs, it is possible to both boost the signal strength and the effective area of the electrode. In addition, Au NPs could enhance the ability of HCT-116 cells to generate reactive oxygen species, leading to the appearance of current spike signals. Therefore, the biosensor in this work can be used to detect the activity of live cells. As a proof-of-concept demonstration, this work highlights this biosensor potential in broad fundamental cell biology studies requiring low costs and ultralow power consumption.

Author contributions

Q. Y. Z. and B. B. H. completed all experiments in device fabrication. Q. Y. Z. and L. R. C. completed all device measurements and the corresponding data collections and analyses. Y. K. Z. conceived the idea. Y. K. Z., Z. X. W. and J. Y. Z. guided the work. Y. K. Z. and L. R. C. completed the mechanism study. L. R. C., J. Y. Z., and Y. K. Z. wrote the original draft of this work. Y. K. Z., J. Y. Z. and Z. X. W. carried out the funding acquisition and project administration. L. R. C., J. Y. Z., Y. B. W. and B. B. H. carried out the methodology and visualization of this work. L. R. C., Q. Y. Z. and Y. B. W. performed the investigation. All authors reviewed this manuscript.

Conflicts of interest

The authors have no conflicts to disclose.

Data availability

The data that support the findings of this study are available from the corresponding authors upon reasonable request.

Supplementary information (SI) is available. See DOI: https://doi.org/10.1039/d5lf00339c.

Acknowledgements

This work was financially funded by the National Natural Science Foundation of China (No. 62574213, 62504165), the Suzhou Fundamental Research Project (No. SSD2024003), the Science and Technology Youth Talent Project of Jiangsu Province (No. JSTJ-2024-016), the Guangdong Basic and Applied Basic Research Foundation (No. 2025A1515012907), and the Students Innovation and Entrepreneurship Foundation of USTC (No. XY2025G002, CY2025X019A). The authors are thankful for the technical support from the Nano-X, Nanofabrication Facility (SNFF) and Characterization & Test platform of SINANO, CAS.

References

1 X. Wang, P. Zhao and Q. Li, *et al.*, Research advances in semiconductor synthetic biology, *Huagong Xuebao*, 2021, **72**(05), 2426–2435, https://link.cnki.net/urlid/11.1946.TQ.20210121.1311.002.

2 J. Liu, Research of Electrochemical Cytosensor Based on Functional Nanamaterials, *PhD dissertation*, Southeast University, 2019, DOI: 10.27014/d.cnki.gdnau.2019.000912.

3 C. Kang, K. L. Shrestha and S. Kwon, *et al.*, Intein-Mediated Protein Engineering for Cell-Based Biosensors, *Biosensors*, 2022, **12**(5), 283, DOI: 10.3390/bios12050283.

4 Y. Vakhovskyi, D. Mruga and O. Ustinov, *et al.*, Design and Optimization of Biosensor for Pyruvate Quantification, *Electroanalysis*, 2025, **37**(10), e70064, DOI: 10.1002/elan.70064.

5 G. Koohkansaadi, A. Mohagheghi and A. Mobed, *et al.*, Emerging Biosensor Technologies for Stroke Biomarker Detection: A Comprehensive Overview, *Anal. Sci. Adv.*, 2025, **6**(2), e70035, DOI: 10.1002/ansa.70035.

6 P. Sharma, J. Harberts and R. Sánchez-Salcedo, *et al.*, Implantable, Label-Free NIR-Based Porous Silicon Biosensor for Monitoring Biomarkers in Interstitial Fluid, *Adv. Sens. Res.*, 2025, e00007, DOI: 10.1002/adsr.202500007.

7 L. Zhu, X. Lan and X. Xiao, *et al.*, Structure Switchable Single Fluorophore Biosensor to Measure Dissociation Constant in PAT Aptamer Tailoring, *Small*, 2025, **21**(30), 2504007, DOI: 10.1002/smll.202504007.

8 F. Cui, Y. L. Liu and X. C. Wang, *et al.*, Eu_6-Cluster-Based Metal–Organic Framework Biosensor for Sensitive Luminescence Detection of Catecholamine Metabolites, *Appl. Organomet. Chem.*, 2025, **39**(9), e70341, DOI: 10.1002/aoc.70341.

9 J. Sun, L. Zhou and Z. Li, *et al.*, Perovskite-Graphene Heterostructure Biosensor Integrated with Biotunable Nanoplasmonic Ternary Logic Gate for Ultrasensitive Cytokine Detection, *Adv. Sci.*, 2025, **12**(29), e03124, DOI: 10.1002/advs.202503124.

10 Q. Liu, C. Wu and H. Cai, *et al.*, Cell-Based Biosensors and Their Application in Biomedicine, *Chem. Rev.*, 2014, **114**(12), 6423–6461, DOI: 10.1021/cr2003129.

11 D. Özsoylu, T. Wagner and M. J. Schöning, Electrochemical Cell-based Biosensors for Biomedical Applications, *Curr. Top. Med. Chem.*, 2022, **22**(9), 713–733, DOI: 10.2174/1568026622666220304213617.

12 A. Alikhani, M. Gharooni and H. Moghtaderi, *et al.*, An electrochemical biosensor to distinguish between normal and cancer cells based on monitoring their acidosis using gold-coated silicon Nano-roughened electrode, *Anal. Biochem.*, 2018, **561–562**, 1–10, DOI: 10.1016/j.ab.2018.09.005.

13 S. Chen, P. Zhao and L. Jiang, *et al.*, Cu_2O-mediated assembly of electrodeposition of Au nanoparticles onto 2D metal-organic framework nanosheets for real-time monitoring of hydrogen peroxide released from living cells, *Anal. Bioanal. Chem.*, 2020, **413**(2), 613–624, DOI: 10.1007/s00216-020-03032-6.

14 W. Chen, W. Zhang and Z. Lian, *et al.*, Ultrasensitive Electrochemiluminescence Biosensor Based on G-quadruple Structure Targeted with Platinum(II) Complexes for Early Biomarker Detection of Disease, *Adv. Opt. Mater.*, 2025, **13**(29), e01324, DOI: 10.1002/adom.202501324.

15 K. Niu, The Study of Photolectrochemical Sensors Based on Inorganic Semiconductor Nanomaterials, *Master Thesis*, Northeastern University, 2017.

16 K.-M. Koo, C.-D. Kim and F. N. Ju, *et al.*, Recent Advances in Electrochemical Biosensors for Monitoring Animal Cell Function and Viability, *Biosensors*, 2022, **12**(12), 1162, DOI: 10.3390/bios12121162.

17 A. Poghossian and M. J. Schöning, Label-Free Sensing of Biomolecules with Field-Effect Devices for Clinical Applications, *Electroanalysis*, 2014, **26**(6), 1197–1213, DOI: 10.1002/elan.201400073.

18 J. Liu, K. Liu and X. Liu, *et al.*, Self-Powered Biosensor Driven by a Hybrid Biofuel Cell with CuCoP-Polyoxometallate Composite as Both Cathode Catalyst and Sensing Interface, *Small*, 2025, **21**(30), 2500451, DOI: 10.1002/smll.202500451.

19 W. Lei, S. Zhang and J. Shu, *et al.*, Self-Powered Glucose Biosensor Based on Non-Enzymatic Biofuel Cells by Au Nanocluster/Pd Nanocube Heterostructure and Fe_3C@C-Fe Single-Atom Catalyst, *Small*, 2025, **21**(13), 2410326, DOI: 10.1002/smll.202410326.

20 I. Shitanda, T. Samori and M. Satake, *et al.*, Wearable Self-Powered Biosensor for Continuous Lactate Monitoring in Sweat, *ChemElectroChem*, 2025, **12**(20), e202500222, DOI: 10.1002/celc.202500222.

21 J. Hopkins, K. Fidanovski and A. Lauto, *et al.*, All-Organic Semiconductors for Electrochemical Biosensors: An Overview of Recent Progress in Material Design, *Front. Bioeng. Biotechnol.*, 2019, **7**, 237, DOI: 10.3389/fbioe.2019.00237.

22 Y. He, K.-Y. Chen and T.-T. Wang, *et al.*, MiRNA-155 Biosensors Based on AlGaN/GaN Heterojunction Field Effect Transistors With an Au-SH-RNA Probe Gate, *IEEE Trans. Electron Devices*, 2023, **70**(4), 1860–1864, DOI: 10.1109/ted.2023.3245569.

23 A. Podolska, S. Tham and R. D. Hart, *et al.*, Biocompatibility of semiconducting AlGaN/GaN material with living cells, *Sens. Actuators, B*, 2012, **169**, 401–406, DOI: 10.1016/j.snb.2012.04.015.

24 Y. Hou, J. Jing and Y. Luo, *et al.*, A Versatile, Incubator-Compatible, Monolithic GaN Photonic Chipscope for Label-Free Monitoring of Live Cell Activities, *Adv. Sci.*, 2022, **9**(17), 2200910, DOI: 10.1002/advs.202200910.

25 Y. Zhao, X. Fang and X. Yan, *et al.*, Nanorod arrays composed of zinc oxide modified with gold nanoparticles and glucose oxidase for enzymatic sensing of glucose. Article, *Microchim. Acta*, 2015, **182**(3-4), 605–610, DOI: 10.1007/s00604-014-1364-9.

26 S. Mehmood, R. Ciancio and E. Carlino, *et al.*, Role of Au(NPs) in the enhanced response of Au(NPs)-decorated MWCNT electrochemical biosensor. Article, *Int. J. Nanomed.*, 2018, **13**, 2093–2106, DOI: 10.2147/ijn.S155388.

27 J. Zhu, Z. Ye and X. Fan, *et al.*, A highly sensitive biosensor based on Au NPs/rGO-PAMAM-Fc nanomaterials for detection of cholesterol. Article, *Int. J. Nanomed.*, 2019, **14**, 835–849, DOI: 10.2147/ijn.S184013.

28 L. Qiang, Y. Zhang and X. Guo, *et al.*, A rapid and ultrasensitive colorimetric biosensor based on aptamer functionalized Au nanoparticles for detection of saxitoxin. Article, *RSC Adv.*, 2020, **10**(26), 15293–15298, DOI: 10.1039/d0ra01231a.

29 M. Jiang, Y. Zhao and L. Bian, *et al.*, Realizing bidirectional photocurrent in monolithic dual-mode device for neuromorphic vision and logically-encrypted transmission, *Adv. Funct. Mater.*, 2025, **35**(19), 2570106, DOI: 10.1002/adfm.202570106.

30 J. Zhang, J. Li and L. Yang, *et al.*, Electric-stimulated controllable synaptic GaN nanodevice for neuromorphic computing, *Chip*, 2025, **4**(4), 100149, DOI: 10.1016/j.chip.2025.100149.

31 S. M. A. Haghparast, T. Kihara and J. Miyake, Distinct mechanical behavior of HEK293 cells in adherent and suspended states, *PeerJ*, 2015, **3**, e1131, DOI: 10.7717/peerj.1131.

32 E. R. Travis and R. M. Wightman, Spatio-temporal resolution of exocytosis from individual cells. Review, *Annu. Rev. Biophys. Biomol. Struct.*, 1998, **27**, 77–103, DOI: 10.1146/annurev.biophys.27.1.77.

33 A. Maddah, H. Danesh and N. Ziamajidi, *et al.*, Oxidative Stress Induction by Gold Nanoparticles in HCT-116 Colon Cancer Cells, *Comprehensive Health and Biomedical Studies*, 2024, **2**(1), e145183, DOI: 10.5812/chbs-145183.

34 R. Liu and D. Wang, Tunneling Electron Transfer across Cell Membrane via Au Nanoparticles in Single Living Cells, *Nano Lett.*, 2024, **24**(8), 2451–2456, DOI: 10.1021/acs.nanolett.3c03928.

35 G. S. Mishra, N. Mohankumar and S. K. Singh, Impact of InGaN notch on sensitivity in dielectric modulated dual channel GaN MOSHEMT for label-free biosensing, *Curr. Appl. Phys.*, 2023, **49**, 83–90, DOI: 10.1016/j.cap.2023.01.014.

36 C. H. Chen, E. R. Ravenhill and D. Momotenko, *et al.*, Impact of Surface Chemistry on Nanoparticle-Electrode Interactions in the Electrochemical Detection of Nanoparticle Collisions, *Langmuir*, 2015, **31**(43), 11932–11942, DOI: 10.1021/acs.langmuir.5b03033.

37 S. M. Lu, M. Y. Li and Y. T. Long, Dynamic Chemistry Interactions: Controlled Single-Entity Electrochemistry, *J. Phys. Chem. Lett.*, 2022, **13**(21), 4653–4659, DOI: 10.1021/acs.jpclett.2c00960.

38 S. Freko, L. J. K. Weiss and F. C. Simmel, *et al.*, Direct Single-Impact Electrochemistry Using Silver Nanoparticles as a "Digital" Readout for Biosensing Applications, *ACS Sens.*, 2025, **10**(6), 3840–3853, DOI: 10.1021/acssensors.5c00064.